

ChemComm

Accepted Manuscript



This is an *Accepted Manuscript*, which has been through the Royal Society of Chemistry peer review process and has been accepted for publication.

Accepted Manuscripts are published online shortly after acceptance, before technical editing, formatting and proof reading. Using this free service, authors can make their results available to the community, in citable form, before we publish the edited article. We will replace this *Accepted Manuscript* with the edited and formatted *Advance Article* as soon as it is available.

You can find more information about *Accepted Manuscripts* in the [Information for Authors](#).

Please note that technical editing may introduce minor changes to the text and/or graphics, which may alter content. The journal's standard [Terms & Conditions](#) and the [Ethical guidelines](#) still apply. In no event shall the Royal Society of Chemistry be held responsible for any errors or omissions in this *Accepted Manuscript* or any consequences arising from the use of any information it contains.

Cite this: DOI: 10.1039/c0xx00000x

www.rsc.org/xxxxxx

Communication

Two-dimensional g-C₃N₄: an ideal platform for examining facet selectivity of metal co-catalysts in photocatalysis†

Song Bai, Xijun Wang, Canyu Hu, Maolin Xie, Jun Jiang* and Yujie Xiong*

Received (in XXX, XXX) Xth XXXXXXXXX 20XX, Accepted Xth XXXXXXXXX 20XX

DOI: 10.1039/b000000x

Two-dimensional g-C₃N₄ nanosheets with few-layer thickness, ensuring equivalent charge migrations to various Pd facets, provide an ideal model system for reliably examining the facet selectivity of Pd co-catalysts. It reveals that reduction of CO₂ can better occur on Pd{111} facets while H₂O prefers to generate H₂ on Pd{100}.

Photocatalysis is a process involving the photo-excitation of semiconductor materials to generate electron-hole pairs, and in turn, the migrations of electrons and holes to different sites for redox reactions.¹ In conversion of CO₂ and H₂O into carbon fuels, photo-generated electrons transfer to CO₂ species at the material surface for reduction, accompanied by reception of holes by H₂O molecules at another site for oxidation.² However, the H₂O molecules also have the chance to pick up electrons from the reduction sites to generate H₂, and such a water splitting process constitutes a competition with the reduction of CO₂.^{2a} Thus reduction selectivity (i.e., the relative activity of CO₂ to H₂O in the reduction) is crucial to solar-to-chemical energy conversion. In the past years, metal co-catalysts have been widely used to facilitate charge separation in semiconductor by taking advantage of Schottky junction,³ and collect electrons at their surface for the reduction. In the hybrid configuration, the electrons and holes are accumulated on two different materials so that the reduction can be well spatially separated from the oxidation. As such, it becomes feasible to readily tune the reduction selectivity by tailoring the metal component.

As demonstrated in many other reactions, the surface facets of metal catalysts have a huge impact on the molecular adsorption and activation.⁴ For this reason, the facet design of metal co-catalysts holds the promise for tuning the reaction selectivity in photocatalysis. In analyzing the surface-molecule interactions, the charge density in the metal co-catalysts, which depends on the efficiency of charge transfer from semiconductor to metal, has to be taken into account. In order to investigate the facet-dependent reaction selectivity, it is imperative to ensure the system free of variations in this charge-transfer efficiency while maneuvering the surface facets of metal co-catalysts. In most cases, the efficiency of charge migrations from bulk semiconductor to metal surface is varied by the alteration of metal facets due to different couplings of their electronic structures, causing a big concern on the related investigations.

In this communication, we demonstrate that two-dimensional (2D) graphitic-phase C₃N₄ (g-C₃N₄) nanosheets with few-layer thickness can provide an ideal platform to ease this concern. The g-C₃N₄ is an n-type semiconductor with a bandgap of 2.7 eV working in visible spectral region.⁵ The charges generated in 2D semiconductor can easily reach semiconductor-metal interface without the need of traveling through the bulk like traditional three-dimensional (3D) semiconductor. Furthermore, the conjugated structure of g-C₃N₄ may offer multiple coupling configurations with a metal plane, ensuring equivalent efficiency of charge transfer with different Pd surface facets.

The synthetic procedures for g-C₃N₄-Pd hybrid structures with various Pd surface facets are illustrated in ESI,† Fig. S1. The g-C₃N₄ consists of C-N layers connected by weak van der Waals force,^{5b} so bulk g-C₃N₄ powder (ESI,† Fig. S2) can be exfoliated into ultrathin C₃N₄ nanosheets by sonication. Differently from the exfoliation by pure water or isopropanol (IPA) in literature,⁶ a water-IPA cosolvent (i.e., 30 wt% IPA) is used in our work to achieve improved exfoliation yield, as the intensity of steric repulsion has a strong correlation with the cosolvent molecular size.⁷ The yielded C₃N₄ nanosheets, which have a thickness of about 2 nm (i.e., about six C₃N₄ layers, ESI,† Fig. S3), can be well dispersed in water to form transparent suspension. Further, we employ a solution-phase method to *in situ* grow single-faceted Pd nanocrystals on the C₃N₄ nanosheets in such suspension. Different facet-selective capping agents are used for various surface facets of Pd in the synthesis: Br⁻ and I⁻ ions can stabilize the Pd{100} facets,⁸ and synergetic use of HCHO and Na₂C₂O₄ helps form the Pd{111} facets.⁹ In the synthesis, PVP is employed as a dual-function agent to reduce Pd precursor with its hydroxyl end groups as well as to stabilize the yielded Pd nanocrystals.¹⁰ As shown in the transmission electron microscopy (TEM) images and energy-dispersive spectroscopy (EDS) mapping profiles (Fig. 1a and b; ESI,† Fig. S4), both samples have the Pd nanocrystals uniformly dispersed on the surface of C₃N₄ nanosheets. The two samples have comparable edge lengths (4-6 nm in average) on the Pd nanocrystals despite their different shapes. To the best of our knowledge, these are the smallest particle sizes for Pd nanocrystals with specific surface facets obtained in aqueous phase thus far, which are anticipated to boost their catalytic performance due to high surface-to-volume ratios. The high-resolution TEM (HRTEM)

images (Fig. 1c and d) reveal that the Pd nanocrystals with cubic and tetrahedral profiles are single crystals enclosed by {100} and {111} facets, respectively. Note that the lattice fringes of C_3N_4 cannot be resolved by the HRTEM, due to its rapid degradation under irradiation of electron beam.^{6b} The phases, compositions and chemical structure of samples have been verified by X-ray diffraction (XRD, ESI,† Fig. S5), X-ray photoelectron spectroscopy (XPS, ESI,† Fig. S6) and Fourier transform infrared spectroscopy (FT-IR, ESI,† Fig. S7).

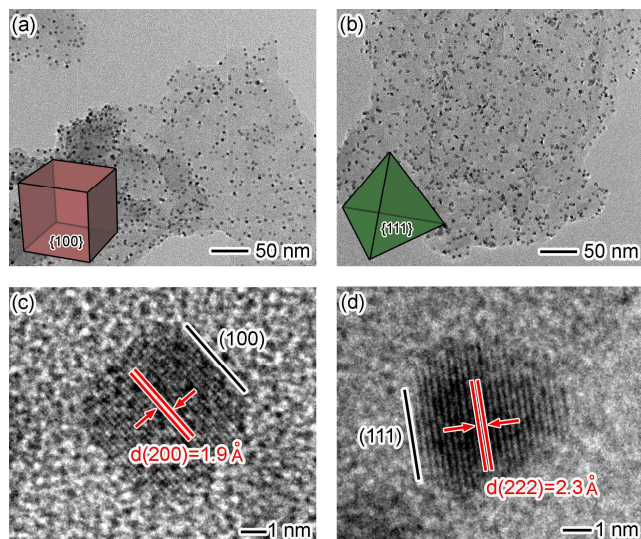


Fig. 1. TEM images of (a) C_3N_4 -Pd nanocubes (NCs) with Pd{100} facets and (b) C_3N_4 -Pd nanotetrahedrons (NTs) with Pd{111} facets. HRTEM images of (c) a Pd NC and (d) a Pd NT on the C_3N_4 nanosheets. Pd loading amounts: 5.7 wt% Pd and 5.8 wt% Pd, respectively.

The C_3N_4 nanosheets that have been deposited with the Pd nanocrystals exhibit similar charge behavior despite their varied surface facets. From the UV-vis diffuse reflectance spectra (ESI,† Fig. S8), it can be seen that the C_3N_4 nanosheets deposited with Pd{100} and Pd{111} nanocrystals show the same bandgap (~2.70 eV) and comparable light absorption. The C_3N_4 -Pd hybrid structures, in reference to bare C_3N_4 nanosheets and bulk C_3N_4 , have been characterized by photocurrent measurements that reflect the efficiency of charge separation in a semiconductor (see Fig. 2a). The measurements show that the addition of Pd to the C_3N_4 nanosheets significantly enhances their photocurrents, suggesting that the C_3N_4 -Pd Schottky junction helps separate photo-generated electron-hole pairs. The nearly equivalent photocurrent enhancements by the Pd{100} nanocubes and Pd{111} nanotetrahedrons indicate that the charge transfer from the C_3N_4 nanosheets to Pd{100} has comparable efficiency from that to Pd{111}, which is further confirmed by their charge-transfer resistance shown in electrochemical impedance spectroscopy (EIS) (ESI,† Fig. S9). This argument is also supported by photoluminescence (PL) emission spectra, which can provide information for the photo-excited charge transfer and recombination processes.¹¹ As shown in Fig. 2b, the PL of C_3N_4 has been substantially quenched with the

addition of Pd. It is an indicator that radiative recombination of electrons and holes has been suppressed by extracting the electrons with the Pd.^{11a} In particular, the PL intensity in the case of Pd nanocubes is analogous to that of nanotetrahedrons, suggesting that both the Pd{100} and Pd{111} can efficiently capture the electrons from the C_3N_4 nanosheets.^{11b}

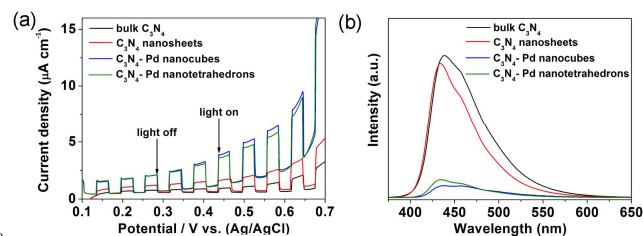


Fig. 2. (a) Photocurrent vs. potential responses of photoelectrodes made of C_3N_4 -Pd hybrid structures and bulk and ultrathin C_3N_4 samples, respectively, at the same C_3N_4 loading weight, measured in a 0.5-M Na_2SO_4 electrolyte under chopped visible-light ($\lambda > 400$ nm) irradiation. (b) PL emission spectra of C_3N_4 -Pd hybrid structures, and bulk and ultrathin C_3N_4 samples (at the same amount of C_3N_4), respectively, excited at 360 nm. In both measurements, Pd loading amounts for the nanocubes and nanotetrahedrons are 5.7 wt% and 5.8 wt%, respectively.

To gain deeper understanding on the probability of charge transfer at C_3N_4 -Pd interface, we have carried out first-principles simulations on the models of C_3N_4 layer and Pd facets (ESI,† Fig. S10a).¹² The computed work function of C_3N_4 (4.31 eV) is lower than those of Pd{100} (5.05 eV) and Pd{111} (5.23 eV) surface (ESI,† Fig. S10b). Along with the formation of g- C_3N_4 -Pd contact, the electrons in the semiconductor with lower work function flow into the metal of higher work function, which thereby levels up the potential energy surface at the interface and eventually builds up a n-type Schottky barrier (ESI,† Fig. S10c). Under visible-light irradiation, the electrons receiving photon energy in the g- C_3N_4 continuously flow into the Pd nanocrystals, while the electrons in the Pd cannot migrate back to the semiconductor and become trapped in the Pd. Such an n-type Schottky junction thus boosts the flow of electrons from the C_3N_4 to the Pd and leaves the holes in the C_3N_4 , facilitating the charge separation. The interfacing of C_3N_4 with Pd metal has been examined by projected density of states (PDOS). The coupling and hybridization of C_3N_4 -Pd electronic structures, revealed by the PDOS (ESI,† Fig. S11-13), suggest the nearly identical probability of interfacial charge transfer despite the different Pd facets. These simulations together with the experimental findings above clearly show that the charge transfer behavior is not affected by altering the surface facets of Pd co-catalysts.

We are then in a position to further investigating the facet-dependent selectivity of Pd co-catalysts in the photocatalytic reactions of CO_2 with H_2O . In the reactions, the photocatalysts are irradiated under visible light in the presence of CO_2 and H_2O vapor. As demonstrated by the potential lineups (ESI,† Fig. S10b), the photo-excited electrons are extracted to the Pd in such a Schottky junction, so the Pd should be the reduction sites in the hybrid C_3N_4 -Pd

Cite this: DOI: 10.1039/c0xx00000x

www.rsc.org/xxxxxx

Communication**Table 1.** Photocatalytic reduction selectivity of CO₂ to H₂O over C₃N₄-based catalysts.^a

catalyst	Pd loading (wt%) ^b	Pd average size (nm) ^c	product rate (μmol g _{cat} ⁻¹ h ⁻¹)				selectivity for CO ₂ reduction (%) ^d	
			H ₂	CO	C ₂ H ₅ OH (×10 ⁻¹)	CH ₄ (×10 ⁻¹)		
1	none	—	—	n.d. ^e	n.d.	n.d.	—	
2	bulk C ₃ N ₄	—	—	1.7	0.1	2.3	n.d.	46.5
3	C ₃ N ₄ NSs	—	—	2.3	0.7	4.0	n.d.	57.4
4	C ₃ N ₄ -Pd NCs	2.9	4.0	25.6	3.3	5.7	n.d.	20.8
5	C ₃ N ₄ -Pd NCs	5.7	4.5	34.1	4.9	6.7	n.d.	20.7
6	C ₃ N ₄ -Pd NCs	11.9	5.9	39.8	5.6	7.4	n.d.	20.1
7	C ₃ N ₄ -Pd NTs	3.1	4.2	8.2	15.4	19.3	0.7	76.9
8	C ₃ N ₄ -Pd NTs	5.8	4.9	9.7	20.3	21.8	2.8	78.1
9	C ₃ N ₄ -Pd NTs	11.6	5.8	6.5	14.9	17.2	1.8	80.0
10 ^f	C ₃ N ₄ -Pd NCs	5.7	4.5	22.2	n.d.	n.d.	n.d.	—
11 ^f	C ₃ N ₄ -Pd NTs	5.8	4.9	7.9	n.d.	n.d.	n.d.	—

^a Reaction conditions: photocatalysts, 10 mg; CO₂ pressure, 0.15 MPa; H₂O, 3.0 mL; irradiation time, 4 h. ^b Pd loading was determined by inductively-coupled plasma mass spectrometry (ICP-MS). ^c See Fig. S15. ^d Selectivity was evaluated on an electron basis (see "Photocatalytic measurements"). ^e Not determined. ^f Using Ar instead of CO₂. The NSs, NCs and NTs denote nanosheets, nanocubes and nanotetrahedrons, respectively. The formation of O₂ was also observed during the reactions.

photocatalysts.¹ Ideally, the CO₂ molecules are reduced to various carbon products such as CH₄, C₂H₅OH and CO by the photo-excited electrons collected at the metal surface, while the H₂O picks up the holes from the semiconductor to generate O₂.² As shown in Table 1 (also ESI,† Table S1), the addition of Pd to the C₃N₄ nanosheets yields reduction products with larger amounts, which can be attributed to better charge separation enabled by the C₃N₄-Pd Schottky junction. However, the H₂O molecules may also simultaneously receive the electrons from the reduction sites (i.e., the metal in the hybrid) to produce H₂ as a side reaction, and as such, the reaction selectivity becomes a critical factor to the reduction of CO₂. It turns out that the selectivity of CO₂ to H₂O in the reduction strongly depends on the shapes of Pd nanocrystals on the C₃N₄ nanosheets (Table 1 and ESI,† Fig. S14). The selectivity by the Pd nanotetrahedrons is significantly higher than that by the nanocubes (*ca.* 80% versus 20%).

In order to identify the origin of reaction selectivity, we have synthesized C₃N₄-Pd hybrid structures with different sizes of Pd nanocrystals that are tuned by adjusting the loading amounts of Pd (ESI,† Fig. S15 and S16). The photocatalytic measurements show that the reaction selectivity is not dependent on the Pd particle sizes as long as the surface facets of Pd nanocrystals are kept the same (Table 1). Given that the ratio of corners/edges to faces has a strong correlation with the particle size, this observation excludes the possibility that the atoms at corners and edges play the key role in activating the CO₂ and H₂O molecules. Thus we can conclude that the faces of Pd nanocrystals are the main sites for the reduction and hold the key to the reaction selectivity. In other words, the CO₂ and H₂O molecules prefer to being reduced on Pd{111} and Pd{100} facets, respectively. This feature has been further verified by the measurements in the absence of

CO₂, which shows higher production rates of H₂ on Pd{100} (Table 1). Note that capping agents have been carefully removed prior to the photocatalysis (ESI,† Photocatalytic measurements). Our experiments reveal that the hybrid structures exhibit excellent shape stability in the photocatalysis (ESI,† Fig. S17), so they can be recycled for further use.

This facet-dependent reaction selectivity can be understood from the viewpoint of molecular adsorption and activation. The molecular behavior on the Pd facets is analyzed by the first-principles theoretical investigations (ESI,† Fig. S18-19). It turns out that the adsorption energy of CO₂ in the case of Pd{111} ($E_a=0.230$ eV) is much higher than that for Pd{100} ($E_a=0.064$ eV), suggesting the better performance of Pd{111} in CO₂ adsorption (ESI,† Fig. S20). The activation energy barriers (E_B) for CO₂ reduction can be obtained from the simulated potential energy surfaces regarding to the variation of C-O bond length. When 2 electrons are brought to the Pd{100} and Pd{111} (which are required to initiate CO₂ activation), the activation barrier E_B can be lowered from 6.79 to 4.15 eV and from 7.15 to 3.98 eV, respectively, demonstrating Pd{111} as a better CO₂ reduction facet. Similar examinations have been carried out for H₂O molecules on Pd{100} and Pd{111} facets (ESI,† Fig. S21). The adsorption of H₂O to Pd{100} ($E_a=0.554$ eV) is significantly stronger than that to Pd{111} ($E_a=0.371$ eV). It makes the Pd{100} better for the H₂O reduction, despite the lower activation barrier for O-H bonding on the Pd{111} charged with 1 electron.

In conclusion, we have demonstrated that reduction of CO₂ can better occur on Pd{111} facets while H₂O prefers to generate H₂ on Pd{100}, by taking advantage of the unique structure of g-C₃N₄ nanosheets. This study provides reliable information for investigating the facet-dependent selectivity

in photocatalytic reactions, opening the door to designing high-selectivity photocatalysts. The research strategy presented here intuitively can be extended to the investigation on material-molecule interactions in other reaction systems.

The authors acknowledge the financial support from the 973 Program (No. 2014CB848900), the NSFC (No. 21101145, 91221104), the Recruitment Program of Global Experts, the CAS Hundred Talent Program, and the Fundamental Research Funds for the Central Universities (No. WK2060190025).

Notes and references

Hefei National Laboratory for Physical Sciences at the Microscale, Collaborative Innovation Center of Chemistry for Energy Materials, and School of Chemistry and Materials Science, University of Science & Technology of China, Hefei, 230026, P.R. China. Fax: 86 551 63603987; Tel: 86 551 63603987; E-mail: yjxiong@ustc.edu.cn, jiangjl@ustc.edu.cn

The first two authors contributed equally to this work.

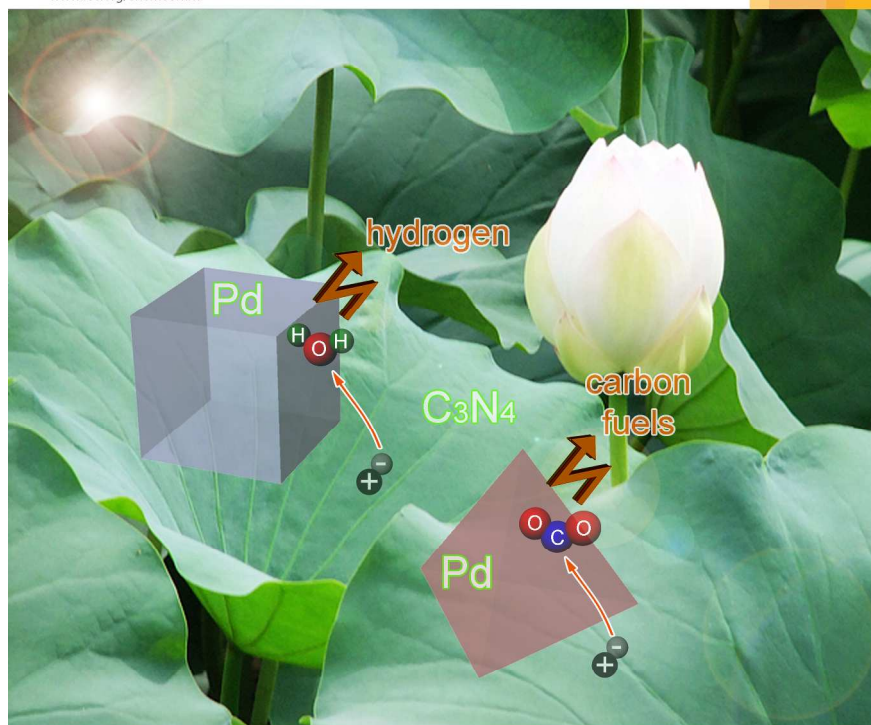
† Electronic Supplementary Information (ESI) available: Detailed experimental procedures and additional characterization data. See DOI: 10.1039/b000000x/

- 1 A. L. Linsebigler, G. Lu and Jr. J. T. Yates, *Chem. Rev.*, 1995, **95**, 735.
- 2 (a) S. C. Roy, O. K. Varghese, M. Paulose and C. A. Grimes, *ACS Nano*, 2010, **4**, 1259; (b) S. N. Habisreutinger, L. Schmidt-Mende and J. K. Stolarczyk, *Angew. Chem. Int. Ed.*, 2013, **52**, 7372; (c) Q. Zhai, S. Xie, W. Fan, Q. Zhang, Y. Wang, W. Deng and Y. Wang, *Angew. Chem. Int. Ed.*, 2013, **52**, 5776.
- 3 J. Yang, D. Wang, H. Han and C. Li, *Acc. Chem. Res.*, 2013, **46**, 1900.
- 4 (a) H. Lee, S. Habas, S. KweSkin, D. Butcher, G. Somorjai and P. Yang, *Angew. Chem. Int. Ed.*, 2006, **45**, 7824; (b) K. M. Bratlie, H.

- Lee, K. Komvopoulos, P. Yang and G. A. Somorjai, *Nano Lett.*, 2007, **7**, 3097; (c) R. Long, K. Mao, X. Ye, W. Yan, Y. Huang, J. Wang, Y. Fu, X. Wang, X. Wu, Y. Xie and Y. Xiong, *J. Am. Chem. Soc.*, 2013, **135**, 3200; (d) C. Wang, H. Daimon, T. Onodera, T. Koda and S. Sun, *Angew. Chem. Int. Ed.*, 2008, **47**, 3588; (e) W. Ong, L. Tan, S. Chai, S. Yong and A. R. Mohamed, *Nanoscale*, 2014, **6**, 1946; (f) W. Ong, L. Tan, S. Chai, S. Yong and A. R. Mohamed, *ChemSusChem*, 2014, **7**, 690; (g) Q. Xiang, J. Yu and M. Jaroniec, *Chem Soc Rev*, 2012, **41**, 782; (h) X. Pan, M. Yang, X. Fu, N. Zhang and Y. Xu, *Nanoscale*, 2013, **5**, 3601; (i) Y. Wang, Q. Wang, X. Zhan, F. Wang, M. Safdar and J. He, *Nanoscale*, 2013, **5**, 8326; (j) D. Y. C. Leung, X. Fu, C. Wang, M. Ni, M. K. H. Leung, X. Wang and X. Fu, *ChemSusChem*, 2010, **3**, 681.
- 5 (a) X. Wang, K. Maeda, A. Thomas, K. Takanahe, G. Xin, J. M. Carlsson, K. Domen and M. Antonietti, *Nat. Mater.*, 2009, **8**, 76; (b) Z. Lin and X. Wang, *Angew. Chem. Int. Ed.*, 2013, **52**, 1735.
- 6 (a) X. Zhang, X. Xie, H. Wang, J. Zhang, B. Pan and Y. Xie, *J. Am. Chem. Soc.*, 2013, **135**, 18; (b) S. Yang, Y. Gong, J. Zhang, L. Zhan, L. Ma, Z. Fang, R. Vajtai, X. Wang and P. Ajayan, *Adv. Mater.*, 2013, **25**, 2452.
- 7 U. Halim, C. Zheng, Y. Chen, Z. Lin, S. Jiang, R. Cheng, Y. Huang and X. Duan, *Nat. Commun.*, 2013, **4**, 2213.
- 8 (a) Y. Xiong, H. Cai, B. Wiley, J. Wang, M. Kim and Y. Xia, *J. Am. Chem. Soc.*, 2007, **129**, 3665; (b) M. Jin, H. Liu, H. Zhang, Z. Xie, J. Liu and Y. Xia, *Nano Res.*, 2011, **4**, 83.
- 9 (a) X. Huang, S. Tang, H. Zhang, Z. Zhou and N. Zheng, *J. Am. Chem. Soc.*, 2009, **131**, 13916; (b) A. Yin, X. Min, Y. Zhang and C. Yan, *J. Am. Chem. Soc.*, 2011, **133**, 3816.
- 10 Y. Xiong, I. Washio, J. Chen, H. Cai, Z. Y. Li and Y. Xia, *Langmuir*, 2006, **22**, 8563.
- 11 (a) J. Yang, H. Yan, X. Wang, F. Wen, Z. Wang, D. Fan, J. Shi and C. Li, *J. Catal.*, 2002, **290**, 151; (b) N. Buehler, K. Meier and J. F. Reber, *J. Phys. Chem.*, 1984, **88**, 3261; (c) M. Tata, S. Banerjee, V. T. John, Y. Waguespack and G. L. McPherson, *Colloids Surf. A*, 1997, **127**, 39.
- 12 G. Kresse and J. Furthmüller, *Phys. Rev. B*, 1996, **54**, 11169.

ChemComm

Chemical Communications
www.rsc.org/chemcomm



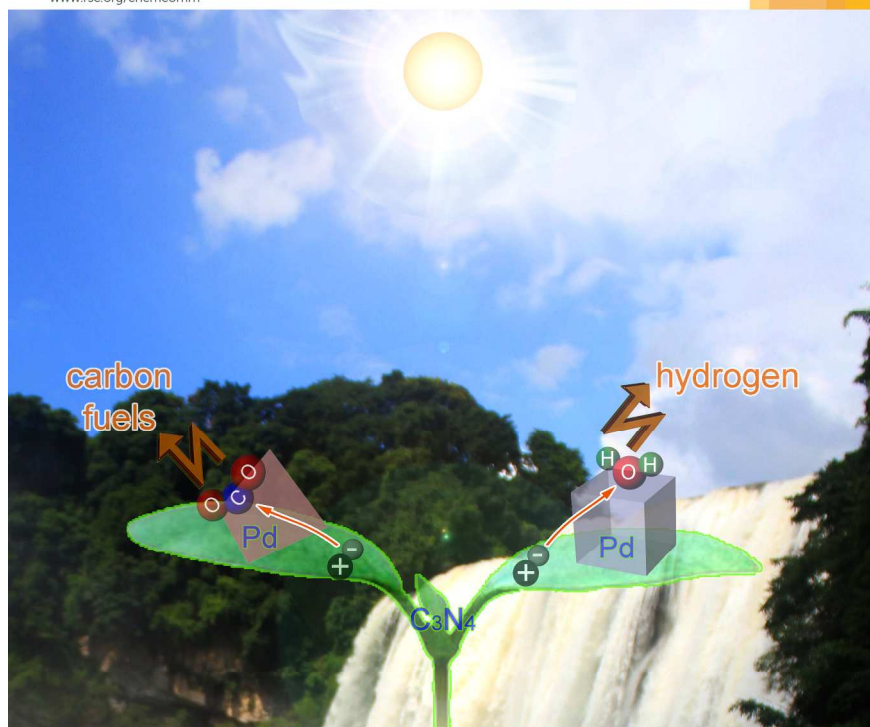
ISSN 1359-7345



213x293mm (300 x 300 DPI)

ChemComm

Chemical Communications
www.rsc.org/chemcomm



ISSN 1359-7345



213x293mm (300 x 300 DPI)